

# Different ocular dominance map formation influenced by orientation preference columns

M.W.Cho & S.Kim

A sia Paci c Center for Theoretical Physics and Nonlinear & Complex Systems Laboratory -NRL,  
D epartment of Physics, P ohang U niversity of Science and Technology, Kyungpook, P ohang, 790-784, K orea

In the mammalian visual cortex, the observed ocular dominance (OD) patterns can be classified as at least three different types. In macaque monkeys, the OD columns form parallel bands of regular spacing with relatively few branching points and mainly oriented perpendicular to area boundaries<sup>1</sup>. The degree of the OD segregation is strong and the average typical spacing of OD,  $\sigma_{OD}$ , is larger than that of orientation preference (OP) columns,  $\sigma_{OP}$  ( $\sigma_{OD} > \sigma_{OP}$ )<sup>2</sup>. In cats, the OD columns form an array of beaded bands exhibiting only a small tendency of elongation perpendicular to area boundaries<sup>3,4</sup>. The degree of OD segregation is intermediate with  $\sigma_{OD} < \sigma_{OP}$ <sup>5</sup>. In the case of tree shrews, the OD segregation is very weak or absent, whereas more stripe-like patterns are observed in extensive OP column regions with low densities of orientation centers, so-called pinwheel centers<sup>6</sup>. Here we will show that such different types of OD segregation are originated by the influence of different interaction strength with the OP columns. We introduce the notion of the anisotropy as a measure of the interaction strength between OD and OP columns using the spin Hamiltonian models. The anisotropy turns out to be crucial in determining the OD map formation types but also influencing on the OP pattern regularity or the pinwheel annihilation rate. We will show that there exist transitions between different OD pattern formation types that depend on the anisotropy. The estimated values of the anisotropy of each species from experimental data are consistent with our predictions. Finally, we discuss why the larger spacing in OD columns in squinters is larger than that of normal animals.

It is well-known that OP and OD patterns in the mammalian visual cortex are not independent, but are correlated<sup>2</sup>. The OP and OD slabs are each aligned with an individual common axis, and these axes found to be orthogonal ("global orthogonality"). The singular points, pinwheel centers, in OP columns tend to align with the centers of OD bands and iso-orientation contours intersect borders of OD bands at right or steep angles ("local orthogonality"). We propose that this correlation between the OP and OD columns is due to the constraint of the normalization of the synapse strength. The orthogonality between the iso-orientation contours and the borders of opposite ocular dominance can be derived from the equilibrium and normalization condition with model independently (see Methods). This constraint has a neurobiological connection to the homeostasis or synapse plasticity rule, that the sum of all the synaptic weights (or of their square values) of synapses impinging on the cell remains constant or a conserved sum of the synaptic weights of all contacts made in the network by the same parent axon<sup>7</sup>. When response properties of cortical cells or small cortical regions at each cortical location  $r$  are represented by a usual feature vector<sup>8</sup>,

$$(r) = (\mathbf{j}_x(r) \cos 2\pi r; \mathbf{j}_y(r) \sin 2\pi r; z(r)) \quad (1)$$

for the preferred orientation  $\theta(r)$ , and the ocular dominance  $z(r)$ , the imposed restriction for normalization is  $\mathbf{j}_x(r)^2 + \mathbf{j}_y(r)^2 + z(r)^2 = 1$  for all  $r$ . Here,  $\mathbf{j}_x(r)$  which measures the orientation selectivity of the average response of neurons, vanishes at pinwheel centers, so that

strong ocular dominance can occur near pinwheel centers from the normalization constraint. Such development of the strong scalar component near the singularity centers of the orientational component due to the normalization constraint are also observed in other physical systems. For example, the (in-plane) vortices, the leading player in superconductors and superuids, are singularities at the orientational components, equivalent to the pinwheel centers in OP columns. The formation of the island structure at the scalar component near the singular centers is known as the development of the out-of-plane vortex in magnetism.

In the context of magnetism, the conventional spin vector  $\mathbf{S}_i = (S_i^x; S_i^y; S_i^z)$  can serve as a useful representation of the feature vector in Eq.(1) with the preferred orientation  $\theta_i = (1/2) \tan^{-1}(S_i^y/S_i^x)$  and the ocular dominance  $S_i^z$ . The visual map formation with lateral interactions can be described by the spin-like Hamiltonian,

$$H = \sum_{i,j} f J_{OP}(r_{ij}) (S_i^x S_j^x + S_i^y S_j^y) + J_{OD}(r_{ij}) S_i^z S_j^z g, \quad (2)$$

where  $J_{\alpha}(r) = ("=2)I_{\alpha}(r)$  ( $\alpha = OP$  or  $OD$ ) are interaction strengths of a Mexican hat type for OP or OD columns. Each component is normalized to a unit modulus ( $S_i^2 = 1$ ) and the maximal activity rate  $j_{max}$  and  $j_{max,az}$  are incorporated into " $_{OP}$ " and " $_{OD}$ ", denoting the learning rate due to the Hebbian rule. The essential ingredients of the neighborhood function  $I_{\alpha}(r)$  of the lateral interaction can be represented by the Mexican hat

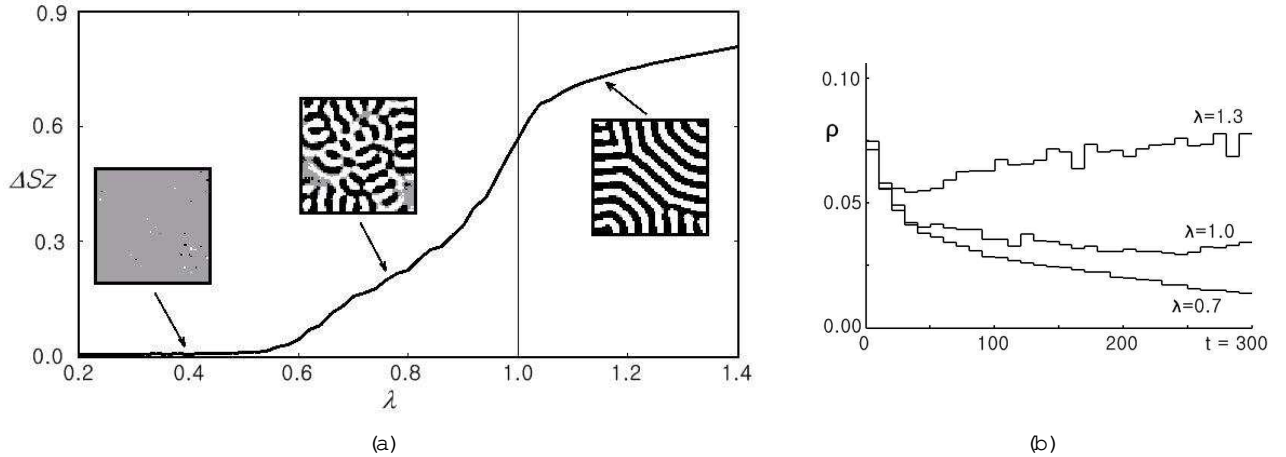


Figure 1: (a) Simulation results of the OD segregation strength and the different OD pattern formation of our model depending on anisotropy. The segregation strength is measured by the standard deviation  $S_z$ , where the region with no segregation ( $S_z = 0.01$ ) is denoted in gray. Simulation conditions are  $J_{OD}^2 = J_{OP}^2 = 6$ ,  $k_{OP} = k_{OD} = 1.0$  ( $J_{OD} = J_{OP}$ ) and the typical spacing of the OD pattern is about  $a_{OD} \approx 8.9$ . Maps are generated using a Metropolis algorithm at zero temperature, with a non-periodic boundary condition and an initially random state in the  $70 \times 70$  lattice, and  $S_z$  is measured at a given time  $t = 100$  and averaged over 10 trial evolutions for a given  $\lambda$ . (b) The pinwheel density  $\rho$  as a function of the development time  $t$  for the anisotropy  $\lambda = 0.7, 1.0$  and  $1.3$ .

type function modified from the wavelet,

$$I(r) = 1 - k \frac{r^2}{2} \exp(-r^2/2) ; \quad (3)$$

where  $k$  is the inhibitory strength and  $r$  is the range of lateral cooperation. Note that we can also use another Mexican hat type function such as the difference of Gaussians (DOG) filters,  $I_{DOG}(r) = \exp(-r^2/2) - k \exp(-r^2/2)$ .

The study of the vortex behaviour in magnetism offer useful hints on our problem of the visual map formation. The classical two-dimensional anisotropic Heisenberg model (CTDAHM), which is applied to superuid  $^3$ He or superconductors, is described by the spin Hamiltontian,

$$H = \sum_{\langle i,j \rangle} K (S_i^x S_j^x + S_i^y S_j^y + S_i^z S_j^z); \quad (4)$$

where  $K > 0$  is the strength of the exchange coupling and the summation  $\langle i,j \rangle$  is done over the neighbors in a lattice. The parameter  $K$  describes the anisotropy of interaction strength between two different components, which in the case of magnetism correspond to in-plane and out-of-plane components. When  $K = 1$ , we get the so-called pure Heisenberg model, which is located at the boundary between two different solutions. For  $K < 1$  (or  $K > 1$ ), the same thermodynamic behaviour is expected to be in the same universality class as the XY (or Ising) model for  $K = 0$  (or  $K = 1$ ) limit. Thermodynamic properties of (4) are well understood in the limit  $K = 0$  following the work of Berezinskii<sup>9</sup> and Kosterlitz and Thouless<sup>10</sup>. It has a phase transition at temperature  $T_{KT}$ , named

the Kosterlitz-Thouless phase transition, which is characterized by a vortex-antivortex unbinding or the stability of isolated vortices. The possibility of two types of vortex solutions (in-plane and out-of-plane) in the two-dimensional anisotropic Heisenberg model was first discussed by Takeno and Hoshina<sup>11</sup> and different values of the critical anisotropy  $c$ , above which out-of-plane vortices are stabilized, were found to exist and depend on the lattice type ( $c = 0.72, 0.82, 0.62$  for square, honeycomb, and triangular lattices, respectively) by Gouvêa et al.<sup>12</sup>

The anisotropy  $\lambda$  in Eq.(2) in the context of Eq.(4) can be interpreted as the ratio of interaction strengths in OP and OD columns, that is,  $J_{OD} = J_{OP}$  or  $J_{OD} = J_{OP}$ . The cooperation ranges also affect the anisotropy parameter. Note that the interaction strength in two-dimension is proportional to the number of interacting pairs  $r^2$ , so that  $J_{OD}^2 = J_{OP}^2$ . The anisotropy can occur also by the difference in the strengths of lateral inhibition  $k$ . The numerical simulation of Eq.(2) reveal the emergence of three different types of OD patterns; (A) for  $\lambda > 1$ , parallel bands patterns with strong OD segregation, (B) for  $\lambda < 1$ , beaded bands patterns with intermediate segregation, and (C) for  $\lambda < c$ , the absence of the OD segregation in the whole region, which correspond to observed patterns in the OD columns of the macaque monkey, the cat and the tree shrew, respectively (Fig. 1(a)). We measure the degree of the OD segregation as the standard deviation of the normalized ocular dominance,  $S_z$  ( $0 \leq S_z \leq 1$ ) at zero temperature and find that the OD segregation strength increases as a function of the anisotropy  $\lambda$ . Three different behaviours in the depen-

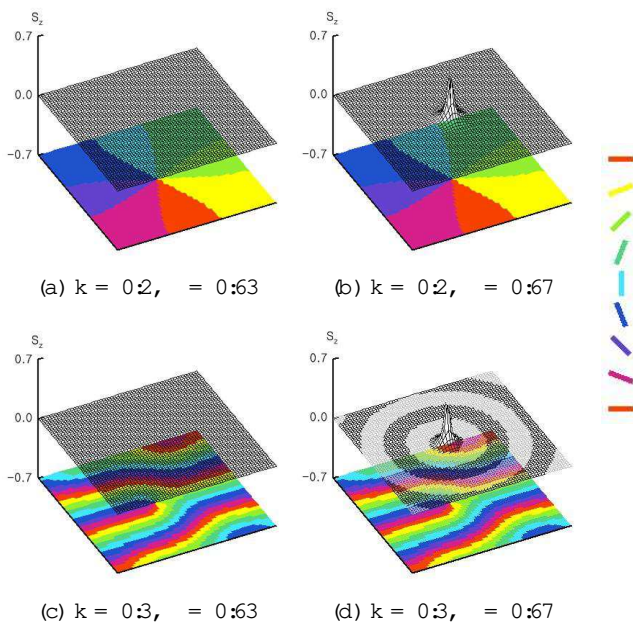


Figure 2: The singularity in the OP column and the development of the peak in OD the column. The simulation is done for our spin Hamiltonian model with initial state with  $\frac{2}{2} = \frac{2}{2} = 6$ ,  $k_{OD} = k_{OP}$  ( $\sigma = "OD" = "OP"$ ), the  $60 \times 60$  lattice size and the non-periodic boundary condition. The colors in OP maps denote the preference angle  $(r)$ . The OD columns ( $S_z$  components) are presented in black and white wired frames, where the black denotes the region with  $S_z(r) = 0$  and white otherwise. A singular point exists either (a) & (b) with a radial extension of the iso-orientation contours for  $k < k_c$  ( $= 1=4$ ) or (c) & (d) with plane-waves for  $k > k_c$ . There exists a threshold  $k_c$ , below which the development of ocular dominance is absent (a) & (c). Above  $k_c$ , a peak emerges in the OD column near the singular point, which decreases monotonously from the singularity center for  $k < k_c$  (b) or display an oscillatory decay for  $k > k_c$  (d).

dence of OD pattern formation on the anisotropy are evidently related to the crossover behaviour of the solutions in the spin Hamiltonian model of the CTDAHM.

In the context of magnetism, the pinwheel annihilation during the visual map development is related to the thermodynamic behaviours of in-plane vortices below the Kosterlitz-Thouless temperature,  $T_{KT}$ . The variation of  $T_{KT}$  with  $\sigma$  is important in magnetism also. Hickam and Tsuneto<sup>13</sup> derived that  $T_{KT}$  decreases monotonously to 0 as  $\sigma$  is increased to 1, which suggest that the pinwheel structures in the OP map last longer or even become stabilized under small thermal fluctuations in the presence of the strong activity in OD columns. Wolf and Geisel first noted that the presence of ocular dominance columns impedes the pinwheel annihilation based on analytic and simulational results<sup>14</sup>. Fig. 1(b) shows the variations of pinwheel densities as a function of development time (x-axis) during the visual map development for different values of the anisotropy. Wolf and Geisel

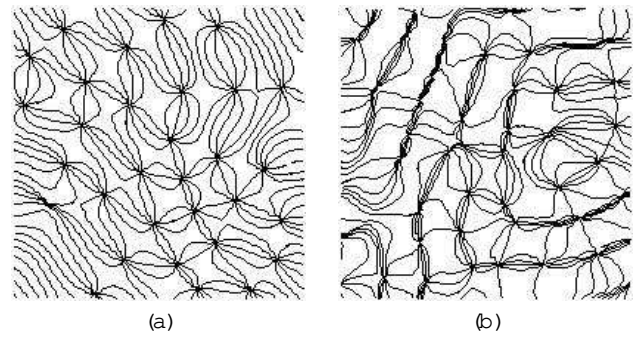


Figure 3: The iso-orientation contours of simulations for (a)  $\sigma = 0.83$  and (b)  $\sigma = 1.38$ . The iso-orientation contours for  $\sigma > 1$  show a much less regular distribution for  $\sigma < 1$ . ( $\sigma = "OD" = "OP"$ ,  $\frac{2}{2} = \frac{2}{2} = 10$ ,  $k_{OP} = k_{OD} = 0.5$  and  $50 \times 50$  lattice size)

showed similar simulational results with the elastic net model using different degrees of OD segregation rather than the anisotropy in our model.

In contrast to the CTDAHM in (4), the spin Hamiltonian for the visual map formation in (2) has inhomogeneous solutions, which produce the emergence of the linear zones in OP maps and the parallel bands in OD maps, if the lateral inhibitory strength  $k$  is larger than a threshold ( $k_c = 1=4$ ). The single vortex simulations in Fig. 2 show the structure of two different vortex types, showing the development of out-of-plane vortices (beaded OD pattern) near the center of in-plane vortices (or pinwheels) in OP maps depending on the anisotropy parameter  $\sigma$ . For  $k < k_c$ , the peak near the orientational singularity in Fig. 2 (b) is a typical feature of in-plane and out-of-plane vortices observed in magnetism. For  $k > k_c$ , vortices exist with plane-wave solutions, which make the linear zones in the OP column and the band structures in the OD column. For  $\sigma > k_c$ , the peak in the ocular dominance column develops near the singularity center in the OP column (Fig. 2 (b) and (d)), which decays sharply away from the center. The emergence of the beaded band pattern in the OD columns of the cat is related to the development of the pulse-shaped out-of-plane components with an oscillatory decay near the singularity in Fig. 2 (d).

For  $\sigma > 1$ , the OD column plays a dominant role in the visual map formation. Parallel bands appear in a whole range of OD columns and make right or steep angle with area boundaries, which is a typical property of the observed OD patterns that are generated without the presence of OP columns. The columnar OP pattern still exist, but are much less regular. The distribution of iso-orientation contours is not uniform with locally dense or sparse region (Fig.3). The angular velocity vector  $\vec{\omega}(r)$  defined in the phase space help to understand this. For

$\sigma = 1$ , the progress in the map formation is balanced between two universal solutions of the XY model or the Ising model. The angular velocity vectors of phase space  $\vec{\omega}$  remain slanted with  $\vec{\omega}_x = \vec{\omega}_y = \vec{\omega}_z = 1=3$  without

falling into the  $S_x - S_y$  plane with the conservation of  $S_z = \frac{1}{\sqrt{1 + f_z^2}} = \frac{1}{\sqrt{2}} = \frac{1}{\sqrt{3}}$ , 0.577 as shown in Fig. 1. For  $f_z > 1$  (or  $< 1$ ), with the rotational plane lying more vertically (or horizontally)  $S_z$  approaches 1 (or 0) as the map formation progresses. If the rotational plane becomes too slanted, the circular trajectory circles are projected to elongated ellipses and lines in the  $S_x - S_y$  plane, leading to irregularities in coordinates.

In the brain *in vivo*, it is not certain which factor among the activity rate  $\alpha$ , the cooperation ranges and the lateral inhibitory strength  $k$  is a major contributor to the anisotropy between OP and OD columns. This may be best answered by comparing the typical spacings  $\alpha_{OP}$  and  $\alpha_{OD}$  that can be measured in the experiments. The typical spacing  $\alpha$  ( $\alpha = OP$  and  $OD$ ) is predicted to be proportional to  $\alpha$  in various models suggested independently<sup>15,16,17</sup>. If the OP and OD columns are different only in the activity rate  $\alpha$ , the typical spacing should be same, that is  $\alpha_{OD} = \alpha_{OP}$  for all  $\alpha$  (see Methods). If they differ only in  $k$ , the typical spacing of OD bands should be smaller than that of OP slabs when the strong OD segregations occurs ( $\alpha_{OD} < \alpha_{OP}$  for  $k > 1$ ). However, if they differ only in  $\alpha$ , the typical spacing of OD bands should be larger than that of OP slabs when the strong OD segregations occurs ( $\alpha_{OD} > \alpha_{OP}$  for  $k > 1$ ). Among these possibilities, the last case is consistent with the experimental data in macaque monkey and cat (Table 1). This leads us to conclude that the main factor in the difference in the OD patterns between them macaque monkey and the cat is the cooperation range between OD and OP columns. The simulations with varying cooperation range  $\alpha$  between the OP and the OD columns yields results that agree well with the experimental data as in Fig. 5. More beaded bands in OD columns emerge near the pinwheels like the visual map of the cat for  $\alpha_{OD} < \alpha_{OP}$  (Fig. 5 (a)), whereas parallel bands in the OD map emerge in a whole range like that of the macaque monkey for  $\alpha_{OD} > \alpha_{OP}$  (Fig. 5 (b)).

The spacing of OD columns in squinting cats is known to be larger than that in normally raised animals<sup>18</sup>. In area 17 of strabismic animals, the spacing of adjacent OD columns is about 20–30% larger compared with that in normally raised cats and resembles the spacing of the iso-orientation domains<sup>19</sup>. The actual mechanism by which squint leads to a larger spacing of OD columns is unknown at present. An interesting fact is that the OD columns of strabismic cats form beaded bands, but the spacing of OD columns is equal or larger than that of OP columns (Table 1). The difference in activity rate  $\alpha$  or the cooperation range  $\alpha$  cannot yield such a visual map pattern. If  $\alpha_{OD}$  of the strabismic cat is larger than that of the normal cat, parallel bands will emerge in the OD column of the strabismic cat. We suggest that the elimination of the correlated activity between the two eyes has an effect on the lateral suppression in the OD column. There are experimental evidence that the development of tangential intracortical connections depends on use-

dependent selection mechanism similar to those in the development of thalamocortical connections<sup>20</sup>. Neurons wire together if they are together and lateral inhibition concentrates in the neighborhood of each neuron for the correlated activity in the normal cat. There exist earlier results on simulations with a lateral connection model showing the variation in the OD wavelength depending on the inhibitory strength<sup>21</sup>. However, we obtain similar results on the wavelength by analytic calculation with the spin Hamiltonian model<sup>17</sup>. We also obtain a similar visual map formation for strabismic cats in simulations for  $k_{OD} < k_{OP}$  (Fig. 5 (c)).

The critical anisotropy  $\alpha_c$ , above which the out-of-plane vortex develops and therefore the ocular dominance pattern develops, depends on the neighborhood function  $J(r)$  for lateral interactions. The exact calculation of the critical anisotropy is also an important problem in magnetism<sup>27</sup>. Though any continuum theory will fail in calculation of  $\alpha_c$  because of the singularity near the vortex core<sup>28</sup>, we extend the method of Wysin to the distance interaction models and built a simulation method to obtain the critical anisotropy precisely for different  $J(r)$ <sup>30</sup>. The critical anisotropy allows the determination of the stability boundary of the out-of-plane vortex in the form of  $\alpha_{OD} > \alpha_{OP} + \alpha_c$ . Since the computed value of the  $\alpha_c$  is small, the region for the beaded band pattern can be described by  $\alpha_{OD} > \alpha_{OP} < 1$  where

$\alpha_c = 0.6$ . This agrees well with the experimental data, where for the cat and the ferret  $\alpha_{OD} = \alpha_{OP} = 0.82$ . Fig. 6 shows the phase diagram of the OD pattern formation in the parameter of the cooperation ranges,  $\alpha_{OP}$  and  $\alpha_{OD}$  in the parameter space of  $\alpha_{OP}$  and  $\alpha_{OD}$ . The region with the beaded band OP pattern lies between the regions of the absent OD segregation and the parallel OD bands. The experimentally derived curves for Macaque monkey, Cat, Ferrets lie well within regions of our predictions.

We would like to note that nearly all proposed development models of the visual cortical map are based on a common set of postulates<sup>31</sup> with a focus on varying cortical orientation rules. However, the common results are the proportional relationship between the typical spacing

and the cooperation range  $\alpha$ , the existence of bifurcation between homogeneous and inhomogeneous states, and the influence of the presence of OD columns on pinwheel annihilation. We demonstrate without model specification that the correlations between two columns occur using the normalization of synapse strength (see Methods). Hossmann et al. pointed out the bifurcation from homogeneous to inhomogeneous states as the cooperation range  $\alpha$  decreases in competitive Hebbian models and suggested a sequential bifurcation scenario which explains the different pattern types through dynamics rearrangement that are bound to the already established columnar patterns<sup>32,33</sup>. Wölf et al. suggested that the larger spacing of OD columns in squint is also due to the different developmental order of OP and OD columns<sup>34</sup>. However, the sequential bifurcation scenario

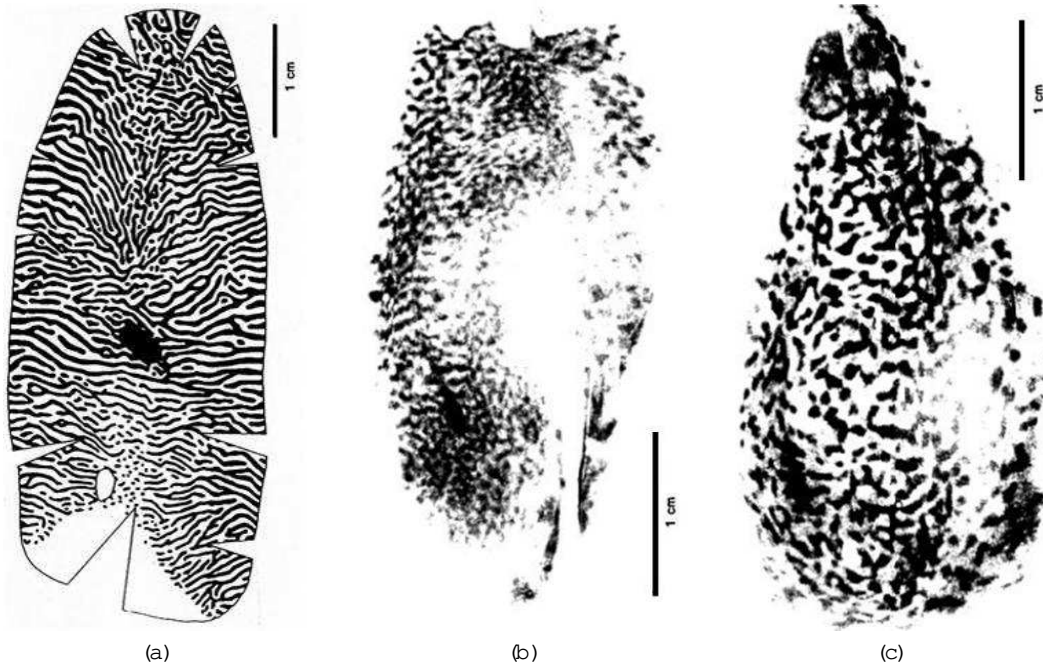


Figure 4: Patterns of OD columns in the visual cortex of (a) the normally raised macaque monkey (ref. 1) (b) the normally raised cat (ref. 18) and (c) a cat raised with artificially induced strabismus (ref. 18). The OD columns in the macaque monkey form parallel bands of regular spacing with relatively few branching points. These bands are mainly oriented perpendicular to area boundaries. The OD columns in both normal and strabismic cats form an array of beaded bands but the periodicity of the OD columns is wider in the strabismic cat (Copyright 1985, 1994 by the Society for Neuroscience).

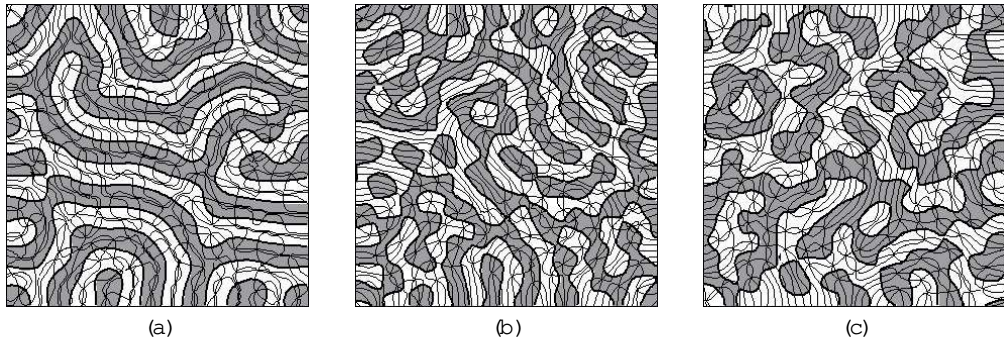


Figure 5: Simulations of OD and OP maps with different typical spacing  $o_P$  and  $o_{OD}$ . (a) Evolution with a larger cooperation range of the OP column than that of the OD column for a normal macaque monkey ( $\frac{2}{o_{OD}} = 13.8$ ,  $\frac{2}{o_P} = 10.0$ ,  $k_{OP} = k_{OD} = 0.7$ ,  $o_{OD} = 11.3$ ,  $o_P = 14.5$ , and  $\frac{2}{o_{OD}} = \frac{2}{o_P} = \frac{2}{o_D} = \frac{2}{o_P} = 1.38$ ) and (b) evolution with larger cooperation range of OD column than that of OP column for normal cat ( $\frac{2}{o_{OD}} = 6.7$ ,  $\frac{2}{o_P} = 10.0$ ,  $k_{OP} = k_{OD} = 0.7$ ,  $o_{OD} = 10.1$ ,  $o_P = 12.4$  and  $o_D = 0.67$ ). The ratio of the cooperation range per each column is according to the experimental data (Table 1). More parallel bands like OD patterns of macaque monkey emerge for  $\frac{2}{o_{OD}} > 1$  (or beaded bands like those of cat for  $\frac{2}{o_{OD}} < 1$ ). (c) Evolution with small inhibitory strength in OD columns for a strabismic cat ( $\frac{2}{o_{OD}} = 6.7$ ,  $\frac{2}{o_P} = 10$ ,  $k_{OD} = 0.35$ ,  $k_{OP} = 0.7$ ,  $o_{OD} = 15.2$ ,  $o_P = 14.5$  and  $o_D = 0.68$ ). Here " $o_{OD}$ " = " $o_P$ " for all cases. The simulations are done on the 100 x 100 lattice size with non-periodic boundary conditions.

is not able to explain the segregation absence in OD columns of tree shrew. We showed that the lateral interaction model has the bifurcation between homogeneous and inhomogeneous states depending on the inhibitory strength  $k$  in lateral interactions rather than the cooperation range  $\alpha$ , not following the sequential bifurcation scenario<sup>17</sup>. Though the anisotropy  $\alpha$  can have various

definitions and its actual values may differ depending on respective models, we believe that the difference in the interaction strength between OP and OD columns determines the type of OD pattern formation without any more complex scheme.

We show that the typical behaviours in the visual map formation are universal. Pinwheels in OP columns or

Table 1: Wavelength of OD and OP columns and OD segregation for different animals

Species	OD [mm]	OP [mm]	$\frac{2}{OD} = \frac{2}{OP}$	$[1/mm^2]$	$\hat{\lambda} = \frac{2}{OP}$	OD pattern	OD segregation
Macaque monkey <sup>a</sup>	0.80	0.68	1.38	8.1	3.75	parallel bands	strong
Normal cat <sup>b</sup>	0.8-1.0	1.0-1.2	0.67	2.1-2.4	2.5-2.9	beaded bands	intermediate
Strabismic cat <sup>c</sup>	1.1-1.3	1.0-1.3	1.1	2.7	3.57	beaded bands	intermediate
Ferret <sup>d</sup>	0.61	0.75	0.66	5.5	2.85	beaded bands	intermediate
Tree shrew <sup>e</sup>		0.52		2.1-2.6			absent

<sup>a</sup> Data from ref. 2. <sup>b</sup> Spacing of OD from ref. 3,18, spacing of OP from ref. 5,22,23 and pinwheel density from ref. 24,25. <sup>c</sup> Data from ref. 19. Lowe et al. 19 used a different algorithm with Rao et al. 24 and Bonhoeffer et al. 25 and obtain average density of pinwheel centers in area 17 of normally raised cats as  $2.6 \text{ pinwheels/mm}^2$ , in the same range as the value observed in strabismic cats. <sup>d</sup> Data of OD from ref. 26 and OP from ref. 24. <sup>e</sup> Data from ref. 6.

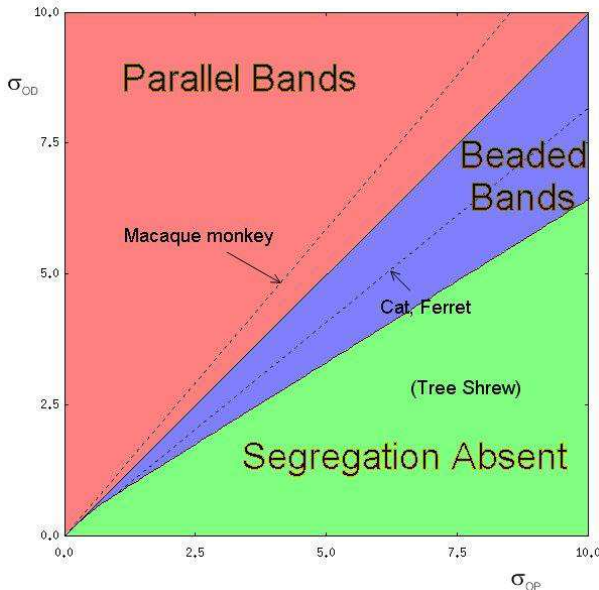


Figure 6: The phase diagram of the ocular dominance patterns according to the cooperation ranges,  $OP$  and  $OD$ , where the experimental data for various animals are also denoted.

beaded band patterns in OD columns are also encountered in other physical systems such as the magnetism but with different. Our proposed method provides a general scheme for reducing the complex process of neural interactions at the cortical level based on a few postulates of the differential geometric idea<sup>17</sup>. We find that a major feature of the visual cortical map formation is not determined by the detailed cortical modality rule but the lattice geometry and the symmetry group in pattern space. We believe that many cortical map formation problems, in particular, in the primary sensory area can be described by our simple approach.

## Methods

Irrespective of the cortical modality rules used, the energy function for the pattern formation should be subject to some constraints. When we perform rotations in the preferred angle by  $(\pi/2 + \theta)$  - called the 'global' gauge transform, the energy function should remain invariant. Moreover, the energy function should be invariant under the reflection  $\theta \rightarrow -\theta$ . Therefore the possible effective Hamiltonian as a function of the preferred angle should take a form of

$$H[\theta] = \frac{1}{2} \int dr^2 (a_2(r) \theta^2 + a_4(r) \theta^4) : \quad (5)$$

The terms with power of  $\theta^3$  and the odd powers of gradient,  $r$  are not present in the energy function. The signs of the parameters  $a_{2n}$  can be determined from the observed pattern *in vivo*:  $(r^2)^2$  term gives the topologic excitations, pinwheels in the orientation column or vortices in magnetism, whose parameter  $a_2$  should be positive. The parameters  $a_{2n}$  for  $n > 2$  should vanish or be positive, otherwise the other types of patterns can emerge in the orientation column. In this case, the lowest order term  $(r^2)^2$  determines the pinwheel formation of the OP map. When the rotation angle  $\theta$  has a dependency on position  $r$ , called the 'local' gauge transform, and the effective Hamiltonian can be rewritten as

$$H[\theta] = a_2 \int dr^2 (r^2 A^2) : \quad (6)$$

The arbitrary vector  $A = \theta(r)$ , called the vector potential in magnetism, is the most important factor in the visual map formation, where the average typical spacing in the OP column is given by  $OP = 2\pi/\lambda$ .  $\lambda$  occurs due to the competitive behaviour between neurons or the inhibitory lateral interactions. If  $\lambda$  vanishes, the linear zones in the OP column cannot be formed. The Hamiltonian in Eq.(6) is a minimal form of the energy function in continuum approximation that can develop two prominent features of the OP columnar pattern formation - emergence of pinwheels and linear zones. The mathematical technique with which the energy function

can be derived by using only the invariant of the transform in the lattice and phase space is well known for physicist as the gauge theory<sup>35</sup>. Similarly, we can get also the effective Hamitonian as a function of the spin components ( $S_x; S_y; S_z$ ), which is related the Lagrangian of the matter field in O(3) or SU(2) symmetry. From the equilibrium condition,  $H = 0$  (or  $H = S = 0$  for  $x, y$  and  $z$ ), we can derive

$$r^2 = 0 \text{ (or } r^2 S = 0\text{)}; \quad (7)$$

which explains the perpendicularity of the iso-orientation contours and the OD bands with the margin of the striate cortex (see ref. 17). From the normalization constraint, we can show

$$r S_x = r S_y = 0 \quad (8)$$

for  $x = 2 \text{ or } y = z$ . The gradient vectors  $r S_x \hat{j}_{x=0}$  and  $r S_y \hat{j}_{y=0}$  denote the normal vectors of iso-orientation contours with  $x = 4, 3 = 4$  and  $y = 0, z = 2$ , which meet perpendicularly at the center of pinwheels. The normal vectors of the borders of opposite ocular dominance,  $r S_z \hat{j}_{z=0}$ , also must meet the iso-orientation contours in steep or right angles from Eq.(8).

The parameters  $a_2$  and  $A$  in Eq.(6) can be decided from the detailed map modelization rules. For our model with the lateral interactions in Eq.(3), we get

$$A_j = \frac{1}{4} \frac{q}{1-k}; \quad (9)$$

with the typical spacing  $k = 2 = A_j$  (see ref. 17). This means that (i) the typical spacing is proportional to the cooperation range and (ii) the linear zones in the OP column or the parallel bands in the OD column can emerge when  $k > 1=4$ . Though, other models also predict similar results with different bifurcation scenarios depending on other factors.

- LeVay, S., Connolly, D. H., Houde, J. & Essén, D. C. V. The complete pattern of ocular dominance stripes in the cortex and visual field of the macaque monkey. *J. Neurosci.* 5, 486-501 (1985).
- Obrein, K. & Blasdel, G. G. Geometry of orientation and ocular dominance columns in monkey striate cortex. *J. Neurosci.* 13, 4114-4129 (1993).
- Lowel, S., Singer, W. The pattern of ocular dominance columns in areas of the cat visual cortex. *Exp. Brain Res.* 68, 661-666 (1987).
- Anderson, P. A., O'laravia, J., & Sluyters, R. C. V. The overall pattern of ocular dominance bands in cat visual cortex. *J. Neurosci.* 8, 2183-2200 (1988).
- Lowel, S., Freeman, B. & Singer, W. Topographic organisation of the orientation column system in large areas of the cat visual cortex: a 2-deoxyglucose study. *J. Comp. Neurol.* 255, 401-415 (1987).
- Bosking, W. H., Zhang, Y., Scheffé, B. R. & Fitzpatrick, D. Orientation selectivity and the arrangement of horizontal connections in tree shrew striate cortex. *J. Neurosci.* 17, 2112-2127 (1997).

- Regnac, Y., Homestasis or synaptic plasticity. *Nature* 391, 845-846 (1998).
- Erwin, E., Obrein, K., & Schultheis, K. Models of orientation and ocular dominance columns in the visual cortex: a critical comparison. *Neural Comput.* 7, 425-468 (1995).
- Berezinskii, V. L. Violation of long range order in one-dimensional and two-dimensional systems with a continuous symmetry group. I. Classical systems. *Zh. Eksp. Teor. Fiz.* 59, 907-920 (1970).
- Kosterlitz, J. M. & Thouless, D. J. Ordering, metastability and phase transitions in two-dimensional systems. *J. Phys. C* 6, 1181-1203 (1973).
- Takeno, S. & Homma, S. Classical spin systems, nonlinear evolution equations and nonlinear excitations. *Prog. Theor. Phys.* 64, 1193-1211 (1980).
- Gouvêa, M. E., Wysin, G. M., Bishop, A. R. & Mertens, F. G. Vortices in the classical two-dimensional anisotropic Heisenberg model. *Phys. Rev. B* 39, 11840-11849 (1989).
- Hikami, S. & Tanemoto, T. Phase transition of quasi-two-dimensional planar system. *Prog. Theor. Phys.* 63, 387-401 (1980).
- Wolf, F. & Geisel, T. Spontaneous pinwheel annihilation during visual development. *Nature* 395, 73-78 (1998).
- Obrein, K., Blasdel, G. G. & Schultheis, K. Statistical-mechanical analysis of self-organization and pattern formation during the development of visual maps. *Phys. Rev. A* 45 7568-7589 (1992).
- Goddard, G. J. & Cimponeriu, A. Analysis of the elastic net model applied to the formation of ocular dominance and orientation columns. *Network*: 11 153-168 (2000).
- Cho, M. W. & Kim, S. Understanding visual map formation through vortex dynamics of spin Hamiltonian models. *Phys. Rev. Lett.* (to be published) arXiv:physics/0306047.
- Lowel, S. Ocular dominance column development: Strabismus changes the spacing of adjacent columns in cat visual cortex. *J. Neurosci.* 14 7451-7468 (1994).
- Lowel, S., Schmidt, K. E., Kim, D. S., Wolf, F., Houssmann, F., Singer, W. & Bonhoefer, T. The layout of orientation and ocular dominance domains in area 17 of strabismic cats. *Eur. J. Neurosci.* 10 2629-2643 (1998).
- Lowel, S. & Wolf, S. Selection of intrinsic horizontal connections in the visual cortex by correlated neuronal activity. *Science* 255 209-212 (1992).
- Sirosh, J. & Mäkkiläinen, R. Ocular dominance and pattern lateral connections in a self-organizing model of the primary visual cortex: Proceeding of the 1994 Neural Information Processing Systems (NIPS) conference.
- Aibus, K. 14C-Deoxyglucose mapping of orientation subunits in the cat's visual cortical areas. *Exp. Brain Res.* 24 181-202 (1979).
- Diao, Y. C., Jia, W., Swindale, N. V. & Cynader, M. S. Functional organization of the cortical 17/18 border region in the cat. *Exp. Brain Res.* 79 271-282 (1990).
- Rao, S. C., Toth, L. J. & Sur, M. Optically imaged maps of orientation preference in primary visual cortex of cats and ferrets. *J. Comp. Neurol.* 387 358-370 (1997).
- Bonhoefer, T., Kim, D. S., Malonek, D., Shoham, D. & Grinvald, A. Optical imaging of the layout of functional domains in area 17 and across the area 17/18 border in cat visual cortex. *Eur. J. Neurosci.* 7 1973-1988 (1995).
- Crowley, J. C. & Katz, L. C. Development of ocular dominance columns in the absence of retinal input. *Nature Neurosci.* 2 1125-30 (1999).

27. Costa, J. E. R. & Costa, B. V. Static and dynam ic simulation in the classical two-dim ensional anisotropic Heisenberg m odel. *Phy. Rev. B* 54 994-1000 (1996).

28. W ysin, W . M . Instability of in-plane vortices in two-dim ensional easy-plane ferrom agnets *Phy. Rev. B* 49 8780-8789 (1994).

29. W ysin, W . M . Critical anisotropies of two-dim ensional magnetic vortices *Phys. Lett. A* 240 95-99 (1998).

30. Cho, M . W . & Kim , S. Instability of planar vortices in two-dim ensional easy-plane Heisenberg m odel with distance- dependent interactions. *arX iv:cond-m at/0310753*.

31. Sw indale, N . V . The development of topography in the visual cortex: a review of m odels. *N etwork*: 7, 161-247 (1996).

32. Ho sum m er, F ., W olf, F ., Geisel, T ., Lowel, S ., & Schmidt, K . Sequential bifurcation of orientation and ocular dominance m aps. In *ICANN 95: P roceedings of the International Conference on Artificial Neural Networks*, volume I, p. 535-540 (EC 2 & C ie, Paris, 1995).

33. Ho sum m er, F ., W olf, F ., Geisel, T ., Lowel, S ., & Schmidt, K . Sequential bifurcation and dynam ic rearrangement of columnar patterns during cortical development. In Jim Bower, editor, *Computation and neural systems* (1996).

34. W olf, F ., Pawelzik, K ., Scherf, O ., Geisel, T . & Lowel, S . How can squint change the spacing of ocular dominance columns? *J. Physiol* 524-537 (2000).

35. Ryder, L. H . *Quantum Field Theory* (Cambridge University Press, 1985).